From kinks to compactonlike kinks

S. Dusuel
Ecole Normale Supérieure de Lyon, 46 Allée d'Italie, 69364 Lyon Cedex 07, France

P. Michaux and M. Remoissenet
Laboratoire de Physique, Université de Bourgogne, 9 Avenue Alain Savary, Boîte Postale 400, 21011, Dijon Cedex, France

(Received 21 July 1997)

We show that, in the continuum limit, the generalized Φ-four or double-well model with nonlinear coupling can exhibit compactonlike kink solutions for some specific velocity regimes and when the nonlinear coupling between pendulums is dominant. Our numerical simulations point out that the static compacton is stable and the dynamic compacton is unstable. Our study is extended to other topological systems where compacton solutions can also be found. A nice feature is that a mechanical analog of the double-well system can be constructed in the form of an experimental lattice of coupled pendulums, which, in the strong coupling limit, allows the observation of these entities. [S1063-651X(98)00502-9]

PACS number(s): 03.40.Kf, 46.30.My

I. INTRODUCTION

Solitary waves and solitons play a significant role in various physical problems. In this context kinks in one-dimensional systems have been used to describe various phenomena such as ferromagnetic [1,2] or ferroelectric domains walls [3], dislocations [4], dynamics of base pairs in DNA macromolecules [5], polymer chain twistings [6] and Josephson junctions [7]. The basic models are generalized Klein-Gordon models where the particles may be considered as coupled to nearest neighbors only, via an interaction potential $U(\theta_{n+1}-\theta_n)$ and subjected to a nonlinear on-site or substrate potential $V(\theta_n)$, where $\theta_n(t)$ is the on-site degree of freedom, which represents the influence of the surrounding lattice atoms and external effects. The lattice Hamiltonian is

$$H=\sum_n \left[\frac{1}{2}\left(\frac{d\theta_n}{dt}\right)^2+U(\theta_{n+1}-\theta_n)+V(\theta_n)\right]. \qquad (1)$$

The corresponding equations of motion can be written in the standard form

$$\frac{d^2\theta_n}{dt^2}-[U'(\theta_{n+1}-\theta_n)-U'(\theta_{n-1}-\theta_n)]+V'(\theta_n)=0. \qquad (2)$$

Depending on the shape of the on-site potential, a nonlinear lattice with the Hamiltonian (1) may sustain different kinds of nonlinear excitations. If $V(\theta_n)$ has two degenerate minima (a double-well shape like in the Φ-four model) or multiple degenerate minima (a periodic shape like in the Frenkel-Kontorova model) topological kink excitations, which connect two equivalent ground states, can exist. If interparticle interactions U' are linear, the kink solutions can be calculated exactly, in the continuum limit [3]; for the discrete equations (2) the kink solutions can be obtained either by perturbation approaches [8] or by numerical techniques. If U' also includes anharmonic interactions, specific kink internal modes may be created [9]. The case where U' is nonlinear only is interesting because of the presence of nonlinear dispersion. Recently it was shown by Rosenau and Hyman [10] that solitary-wave solutions may compactify under the influence of nonlinear dispersion, which is capable of causing deep qualitative changes in the nature of genuinely nonlinear phenomena. Such robust solitonlike solutions, characterized by the absence of the infinite tail, have been called compactons [10,11]. They have been obtained for a special class of the Korteweg–de Vries (KdV)-type equations with nonlinear dispersion. In this paper we would like to show that compactonlike kinks, or compactons for short, can exist for specific velocities in physical systems modeled by a nonlinear Klein-Gordon equation with anharmonic coupling. Part of the motivation of this work finds its origin in the possibility of observing kinks in ''real systems'' with a double-well potential. In this regard, a nice feature is that a mechanical analog can be constructed, allowing one to observe compactons.

The paper is organized as follows. In Sec. II, we show that a generalized Φ-four model with nonlinear coupling may exhibit compacton solutions. We then investigate numerically the existence and stability of these compact entities. Such compactonlike kink solutions can be obtained for other nonlinear topological systems, as presented in Sec. III. In Sec. IV we present an experimental lattice of coupled pendulums which allows us to observe kink solitary waves and compactons. Section V is devoted to concluding remarks.

II. GENERALIZED Φ-FOUR MODEL

A. Analytical results

Consider the generalized Φ-four lattice with on-site potential

$$V(\theta_n)=\frac{V_0}{2}(1-\theta_n^2)^2 \qquad (3)$$

and interaction potential

 © 1998 The American Physical Society

$$U(\theta_{n+1}-\theta_n)=\frac{C_l}{2}(\theta_{n+1}-\theta_n)^2+\frac{C_{\rm nl}}{4}(\theta_{n+1}-\theta_n)^4. \tag{4}$$

Here, V_0, C_l, and $C_{\rm nl}$ are constants that control the potential barrier height of the double well potential and the strength of the linear and nonlinear couplings, respectively. In this case, the equation of motion (2) of the nth particle becomes

$$\frac{d^2\theta_n}{dt^2}=C_l(\theta_{n+1}+\theta_{n-1}-2\theta_n)+C_{\rm nl}[(\theta_{n+1}-\theta_n)^3 + (\theta_{n-1}-\theta_n)^3]+2V_0(\theta_n-\theta_n^3). \tag{5}$$

For $2V_0 \gg C_l$ and $C_{\rm nl}$, θ_n varies slowly from one site to another, and one can use the standard continuum approximation $\theta_n(t)\to\theta(x,t)$ and expand $\theta_{n\pm1}$. Under these conditions, setting $X=x/a$ (that is, measuring the distance x in units of lattice spacing a), Eq. (5) is reduced to

$$\frac{\partial^2\theta}{\partial t^2}-\left[C_l+3C_{\rm nl}\left(\frac{\partial\theta}{\partial X}\right)^2\right]\frac{\partial^2\theta}{\partial X^2}-2V_0(\theta-\theta^3)=0. \tag{6}$$

Equation (6) was obtained by assuming that $3C_{\rm nl}(\partial\theta/\partial X)^2(\partial^2\theta/\partial X^2)\gg(C_l/12)(\partial^4\theta/\partial X^4)$, as will be the case in the following. Note that C_l represents the square of the velocity of linear waves in the chain. For $C_{\rm nl}=0$, Eq. (6) reduces to the standard continuous Φ-four model with linear coupling, which admits tanh-shaped kink solutions.

We then look for localized waves of permanent profile of the form $\theta(s)=\theta(X-ut)$, such as $\theta\to\pm1$ and $d\theta/ds\to0$, when $s\to\pm\infty$, where s is a single independent variable depending on u which is an arbitrary velocity of propagation. Integrating Eq. (6) and taking account of these conditions, we obtain

$$2(u^2-C_l)\theta_s^2-3C_{\rm nl}\theta_s^4+2V_0(1-\theta^2)^2=0. \tag{7}$$

This equation can be integrated for $u^2-C_l=0$, that is, for the two particular cases $C_l=0$ (zero linear coupling: linear waves cannot exist) and $u=0$, and $u=\pm\sqrt{C_l}$, which correspond to kinks with a compact support (see Sec. III) or compactons. One obtains

$$\theta_c(X)=\pm\sin[(2V_0/3C_{\rm nl})^{1/4}(X-X_0)], \tag{8}$$

when $|X-X_0|<1$, and $\theta=\pm1$ otherwise. As usual, the constant of integration (X_0) defines the position of the center of the compacton. For the second case we have

$$\theta(X,t)=\pm\sin[(2V_0/3C_{\rm nl})^{1/4}(s-s_0)], \tag{9}$$

when $|X-\sqrt{C_l}t|<1$, and $\theta=\pm1$ otherwise. Here one has $s=(X-\sqrt{C_l}t)$. From Eqs. (8) and (9) we can calculate the full width of the compactons, which in both cases is equal to $L=\pi(3C_{\rm nl}/2V_0)^{1/4}$. Consequently, when there is no linear coupling one has a static compacton (anticompacton) solution, and, when both linear and nonlinear coupling are present, a dynamic compacton (anticompacton) solution traveling at particular velocity $\sqrt{C_l}$ (or $-\sqrt{C_l}$) may exist. The shape of the dynamic compacton is identical to the shape of the static one; it is represented in Fig. 1(a) for $s_0=0$.

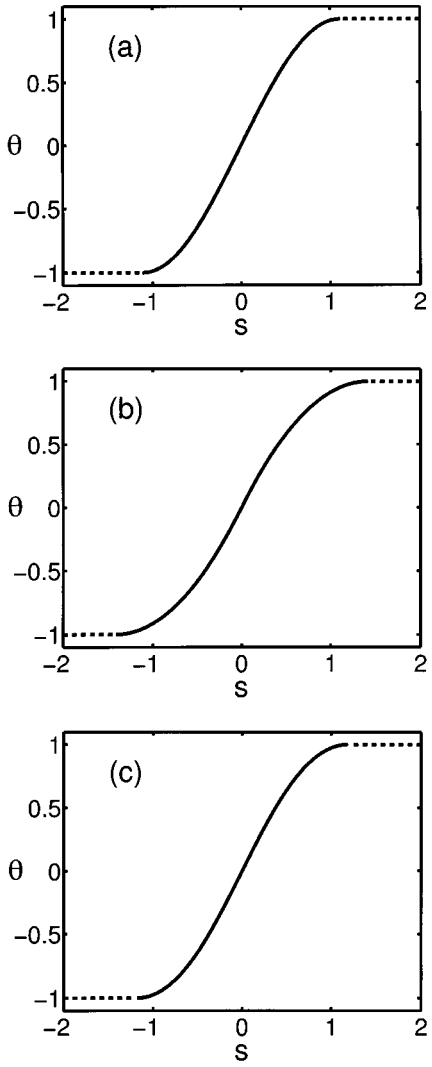

FIG. 1. Representation of field θ (dimensionless) as a function of position s (dimensionless), with $s_0=0$ (compacton center) and $\alpha=1$, corresponding to the wave forms of the compactons for different kinds of on-site potential. (a) Φ-four potential: solution (17). (b) Sinusoidal potential: solutions (19a) and (19b). (c) Double quadratic potential: solutions (21a) and (21b). For each potential the S-shaped wave form (continuous line) represents the compact part which connects the two constant parts ($\theta=\pm1$, horizontal dotted lines) of the solution.

From the continuum approximation of Eq. (1), using Eqs. (3) and (4), one can calculate the total (kinetic plus potential) energy localized in the compacton traveling at velocity $\sqrt{C_l}$. One has

$$E_{\rm tot}=\int_{-\pi/2\gamma}^{\pi/2\gamma}\left[\frac{1}{2}\left(\frac{\partial\theta}{\partial t}\right)^2+\frac{1}{2}C_l\left(\frac{\partial\theta}{\partial X}\right)^2+\frac{1}{4}C_{\rm nl}\left(\frac{\partial\theta}{\partial X}\right)^4 + \frac{1}{2}V_0(1-\theta^2)^2\right]a\,dX, \tag{10}$$

where θ is given by Eq. (8), and we have set $\gamma=(2V_0/3C_{\rm nl})^{1/4}$. After simple calculations, we obtain

$$E_{\mathrm{tot}}=a\gamma\frac{\pi}{2}\left(C_l+\frac{V_0}{2}\right), \tag{11}$$

In the case $u=\sqrt{C_l}=0$, one has

$$E^*_{\mathrm{tot}}=a\gamma V_0\frac{\pi}{4}, \tag{12}$$

which represents the ''mass'' of a static compacton. Note that the energy is strictly localized and contrary to a standard (tanh-shaped) kink, which possesses (exponential) wings and can interact with an antikink, a compacton, and an anticompacton, will not interact unless they come into contact in a way similar to the contact between two hard spheres. Such a result should be interesting for the modeling of static domain walls in condensed matter physics.

B. Numerical results

In order to check the validity of our analytical approach and the stability of our solutions, we performed numerical simulations of the equation of motion (5) which, in the strong coupling (continuous) limit, reduces to Eq. (6). It has been integrated with a fourth-order Runge-Kutta scheme with a time step chosen to preserve the total energy of the system to an accuracy better than 10^{-5} over a complete run.

We first verified the validity of the static compacton ($C_l=0$) solution θ_c given by Eq. (8). If this solution (with parameters $V_0=2$, $L=32a$, and $C_{\mathrm{nl}}=14\,500$) is chosen as an initial condition of the system, and allowed to evolve in the presence of a weak additional dissipation, it relaxes to $\theta=\theta_c+\Delta\theta$, where $\Delta\theta$ are weak spatial sinusoidal deviations from the exact solution with amplitude 4×10^{-4}. Moreover, an arbitrary tanh-shaped initial kink also relaxes toward the same profile θ, proving that θ_c is a good solution to order 10^{-4}. This deviation $\Delta\theta$ from the exact solution can be reduced if we choose a compacton with larger width L, which indicates that the closer to the continuum limit we are, the better the solution is. Actually, this result points out that the static compacton is an exact solution of the continuous system.

For $C_l\neq0$, a dynamic compacton (with parameters $C_l=208$, $V_0=2$, $L=32a$, and $C_{\mathrm{nl}}=14\,500$) launched at initial velocity $\sqrt{C_l}$ emits small radiations. Consequently, its velocity decreases and we no longer have a dynamic compacton as described by solution (9), but rather a kink wave form. It turns out that as soon as they are launched and propagate, dynamic compactons, as described by solution (9), lose their compact shape; they cannot exist. Then, with the same parameters as above, we have analyzed the head-on collision of a compacton (initial velocity $v_i=\sqrt{C_l}$) and an anticompacton (initial velocity $v_i=-\sqrt{C_l}$). Our results, represented in Fig. 2(a), show that the collision is inelastic: the two kinks that emerge from the collision are deformed; they radiate oscillations and propagate at velocities lower than $\sqrt{C_l}$. In Fig. 2(b) we represent the collision between a dynamic compacton (initial velocity $v_i=\sqrt{C_l}$) and a kink (initial velocity $v_i=-0.3\sqrt{C_l}$). Again, two deformed kinks emerge from the collision.

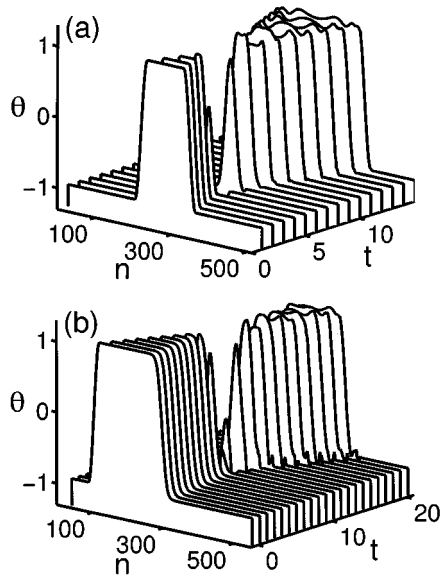

FIG. 2. (a) Inelastic head-on collision (see text) between a compacton traveling initially at velocity $\sqrt{C_l}=14.4$ and an anticompacton travelling initially at velocity $-\sqrt{C_l}$. θ, n, and t are dimensionless. (b) Inelastic head-on collision (see text) between a compacton traveling initially at velocity $\sqrt{C_l}=14.4$ and an antikink traveling initially at velocity $-0.3\sqrt{C_l}$. θ, n, and t are dimensionless.

III. GENERALIZATION TO OTHER MODELS

As we shall see now, compactonlike solutions can be obtained with interaction potential (4), but with different on-site potentials $V(\theta)$. These potentials have two or multiple degenerate minima. We consider three specific potentials: the *ϕ-four potential* (normalized form of the potential considered in Sec. II) $V=(1-\theta^2)^2$, the *sinusoidal (sine-Gordon-type) potential* $V=\frac{1}{2}(1+\cos\pi\theta)$, and the *double quadratic potential* $V=(1-|\theta|)^2$. The equilibrium positions are $\theta=\pm1$, and the barrier height is equal to 1. With an interaction potential U of form (4) and on-site potential $V(\theta)$, in the continuum limit, Eq. (2) may be approximated by

$$\frac{\partial^2\theta}{\partial t^2}-\left[C_l+3C_{\mathrm{nl}}\left(\frac{\partial\theta}{\partial X}\right)^2\right]\frac{\partial^2\theta}{\partial X^2}+V'(\theta)=0. \tag{13}$$

Proceeding as in Sec. II instead of Eq. (7) we obtain

$$2(u^2-C_l)\theta_s^2-3C_{\mathrm{nl}}\theta_s^4+4V(\theta)=0, \tag{14}$$

As in Sec. II we assume $u^2-C_l=0$. Under this, condition (14) becomes

$$\theta_s=[4V(\theta)/\alpha]^{1/4}, \tag{15}$$

where $\alpha=3C_{\mathrm{nl}}$.

We now examine what happens for θ close to 1 (or -1). Let $\theta=1+\varepsilon$, with $|\varepsilon|\ll1$, $\varepsilon\leqslant0$, and $\varepsilon_s\geqslant0$; Eq. (15) can be expanded in terms of ε to give

$$\varepsilon_s=\left[\frac{2}{\alpha}\frac{d^2V}{d\theta^2}\right]^{1/4}\sqrt{-\varepsilon}, \tag{16}$$

where the second derivative is considered at $\theta=1$. Equation (16) can be integrated easily to give

$$\varepsilon(s)=-\frac{1}{4}\left(\frac{2}{\alpha}\frac{d^2V}{d\theta^2}\right)^{1/2}(s-s_0')^2,$$

here s_0' is a constant of integration. For $s=s_0'$, one has $\varepsilon=0$, which is equivalent to $\theta=1$. Thus for $u^2-C_l=0$ the solution is a kink with a compact support or a compacton. Now Eq. (15) can be integrated for the three specific potentials. The results are summarized hereafter.

(i) ϕ-four potential

$$\theta(s)=\sin\left[\left(\frac{4}{\alpha}\right)^{1/4}(s-s_0)\right]. \tag{17}$$

For $\alpha=3C_{\rm nl}$, this normalized solution (where s_0 is a constant of integration) is identical to Eq. (9). It was included here for comparison with the two other potentials.

(ii) Sinusoidal (sine-Gordon type) potential

With this potential, from Eq. (15) one obtains

$$\theta_s=\left(\frac{4}{\alpha}\right)^{1/4}\left(\cos\frac{\pi\theta}{2}\right)^{1/2}, \tag{18}$$

When integrating Eq. (18), we consider two cases: $\theta\geqslant 0$ and $\theta\leqslant 0$, i.e., $s\geqslant s_0$ and $s\leqslant s_0$. Then (from tables of elliptic functions) we obtain

$$\theta(s)=\frac{2}{\pi}\arccos\left\{\mathrm{cn}^2\left[\frac{\pi}{2}\left(\frac{1}{\alpha}\right)^{1/4}(s-s_0),k\right]\right\}\quad \text{for } s\geqslant s_0, \tag{19a}$$

$$\theta(s)=-\frac{2}{\pi}\arccos\left\{\mathrm{cn}^2\left[\frac{\pi}{2}\left(\frac{1}{\alpha}\right)^{1/4}(s-s_0),k\right]\right\}\quad \text{for } s\leqslant s_0. \tag{19b}$$

where cn is a Jacobi elliptic function with parameter $k^2=\frac{1}{2}$.

(iii) Double quadratic potential

In this case, one has

$$\theta_s=(4/\alpha)^{1/4}(1-|\theta|^2)^{1/2}, \tag{20}$$

which is integrated to give

$$\theta(s)=1-\left[1-\frac{1}{2}\left(\frac{4}{\alpha}\right)^{1/4}(s-s_0)\right]^2\quad \text{for } s\geqslant s_0, \tag{21a}$$

$$\theta(s)=-1+\left[1+\frac{1}{2}\left(\frac{4}{\alpha}\right)^{1/4}(s-s_0)\right]^2\quad \text{for } s\leqslant s_0. \tag{21b}$$

The compacton wave form corresponding to each of the above solutions is represented in Figs. 1(a), 1(b), and 1(c) respectively. For each potential the S-shaped wave form (continuous line) represents the compact part which connects the two constant parts ($\theta=\pm 1$; dotted lines) of the solution. We see that although the analytical solutions corresponding to each potential are quite different, the shapes of the compactons look very similar: in fact, they are not very sensitive to the form of potential $V(\theta)$.

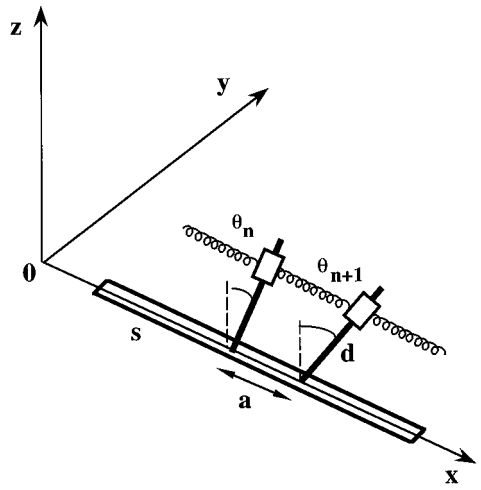

FIG. 3. Sketch of the pendulum lattice apparatus. Here only two pendulums, n and $n+1$, coupled to each other by a spring and attached to the steel ribbon s (parallel to x axis), are represented with their respective angular displacements θ_n and θ_{n+1}. The pendulums are at equilibrium in one of the two equivalent potential wells. The motion can occur in a plane perpendicular to the chain (x axis); see also Fig. 5(a).

IV. MECHANICAL ANALOG

A. Analysis

Analog mechanical systems, such as the experimental mechanical transmission line first introduced by Scott [12], play an important role in the study of kink solitons [13] and their remarkable properties. Thus, in order to observe kinks and compactons, we constructed a mechanical analog which consists of an experimental chain of identical pendulums, as sketched in Fig. 3. Each basic unit is similar to the pendulum recently studied by Peters [14]: it can oscillate with a motion whose character is determined by the forces of torsion and gravity in opposition; for the configuration presently considered it possesses two equilibrium positions (two wells). Each pendulum is connected to its neighbors by springs. When the dissipation is neglected and the difference between angular displacement of neighboring pendulums are small enough, the equation of motion of the nth chain unit is given (see the Appendix) by

$$I\frac{d^2\theta_n}{dt^2}=-K\theta_n+mgd\,\sin\theta_n+C_{0,l}(\theta_{n+1}+\theta_{n-1}-2\theta_n)-C_{0,\rm nl}(\theta_n-\theta_{n+1})^3-C_{0,\rm nl}(\theta_n-\theta_{n-1})^3, \tag{22}$$

where the terms on right hand site represent the restoring torque owing to the torsion, the gravitational torque and the restoring torque owing to the coupling with the neighboring pendulums (see the Appendix). $\theta_n(t)$ is the angular displacement as a function of time t of the nth pendulum, $I=md^2$ is the moment of inertia of a single pendulum of mass m and length d, g is the gravitation, and K is the torsion constant. $C_{0,l}$ and $C_{0,\rm nl}$ are the linear and nonlinear torque constant of a spring between two pendulums: they are given by

$$C_{0,l}=kd^2\left(1-\frac{l_0}{l_1}\right), \tag{23a}$$

$$C_{0,\mathrm{nl}}=kd^2\left(\frac{l_0 d^2}{2l_1^3}-\frac{C_{0,l}}{6}\right) \tag{23b}$$

where k is the spring stiffness, l_0 the natural length of a spring at rest, and l_l the length of this spring when it is stretched between two adjacent pendulums at equilibrium (bottom of one well). Note that the nonlinear coupling term must be fully taken into account because the linear term is especially small when l_l is not very different from l_0. Moreover, when $l_0=l_l$, we have $C_{0,l}=0$ and $C_{0,\mathrm{nl}}=kd^4/2Kl_1^2$, as we will see in the following.

Setting

$$\tau=\frac{K}{I}\,t,\quad \Gamma=\frac{mgd}{K},\quad C_{1,l}=\frac{C_{0,l}}{K},\quad C_{\mathrm{nl}}=\frac{C_{0,\mathrm{nl}}}{K}, \tag{24}$$

we transform Eq. (21) into

$$\frac{d^2\theta_n}{d\tau^2}+\theta_n-\Gamma\ \sin\ \theta_n+C_{1,l}(2\theta_n-\theta_{n+1}-\theta_{n-1})$$
$$+C_{\mathrm{nl}}[(\theta_n-\theta_{n+1})^3+(\theta_n-\theta_{n-1})^3]=0. \tag{25}$$

In Eq. (25), the quantity $(-\theta_n+\Gamma\ \sin\theta_n)$ represents the ''on-site'' (zero coupling limit) torque. In the continuum approximation one obtains

$$\frac{\partial^2\theta}{\partial\tau^2}-\left[C_{1,l}+3C_{\mathrm{nl}}\left(\frac{\partial\theta}{\partial X}\right)^2\right]\frac{\partial^2\theta}{\partial X^2}+\theta-\Gamma\ \sin\theta=0. \tag{26}$$

The on-site potential energy, corresponding to Eq. (26) [or Eq. (25)] is

$$V(\theta_n)=\tfrac{1}{2}(\theta_n^2-\theta_m^2)+\Gamma(\cos\ \theta_n-\cos\theta_m). \tag{27}$$

Here the parameter Γ plays the role of a control parameter. For $\Gamma>1$ it determines the depth and separation of the two wells [14], and $\pm\theta_m$ correspond to the two equilibrium positions. Equation (25) and its continuum approximation (27) cannot be solved analytically. Nevertheless, in order to obtain some approximate solution, one can replace the potential $V(\theta_n)$ by the standard Φ-four potential given by Eq. (3) with $\theta_n\rightarrow\theta_n/\theta_m$ and $V_0=-{\theta_m}^2+2\Gamma(\cos\theta_n-\cos\theta_m)$. As depicted in Fig. 4, the fitting is good for $-\theta_m<\theta_n<\theta_m$. Under these conditions, Eq. (25) reduces to

$$\frac{d^2\Theta_n}{dT^2}+C_l(2\Theta_n-\Theta_{n+1}-\Theta_{n-1})+C_{\mathrm{nl}}[(\Theta_n-\Theta_{n+1})^3$$
$$+(\Theta_n-\Theta_{n-1})^3]-2V_0'(\Theta_n-\Theta_n^3)=0, \tag{28}$$

where $\Theta_n=\theta_n/\theta_m$, $T=\theta_m\tau$, $C_l=C_{1,l}/\theta_m^2$, and $V_0'=2V_0/\theta_m^4$. In the continuum limit, Eq. (28) is approximated by

$$\frac{\partial^2\Theta}{\partial T^2}-\left[C_l+3C_{\mathrm{nl}}\left(\frac{\partial\Theta}{\partial X}\right)^2\right]\frac{\partial^2\Theta}{\partial X^2}-2V_0'(\Theta-\Theta^3)=0. \tag{29}$$

Equations (28) and (29) are similar to Eqs. (5) and (6). Thus Eq. (29) admits compacton solutions of the forms (8) and (9).

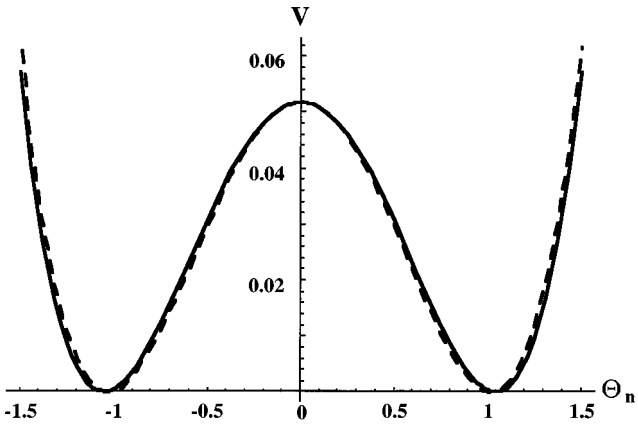

FIG. 4. Fitting of the double-well potential (27): dotted line, by a Φ-four potential of form (3): continuous line. For $-1.5<\theta_n<1.5$ the two curves are practically superimposed and the approximation of the double-well potential of the real system by a Φ-four potential is justified.

B. Apparatus and experiments

The apparatus is a lattice of 20 pendulums attached vertically to the center of a horizontal steel ribbon (2 m long, 6 mm wide, and 0.1 mm thick) supported by vertical metallic plates which are equidistant ($a=10$ cm) (see Figs. 3 and 5). A basic pendulum consists of a thin rod (diameter 3 mm) along which a cylinder (mass $m=67$ g) can be displaced and fixed. Depending on the vertical position d of the mass along the rod, the system can oscillate with a motion which depends on the potential shape, and is determined, as mentioned earlier, by the forces of gravity and torsion in opposition. Here, with $d=87$ mm and $K=0.03$, the control parameter is $\Gamma=1.9$, thus the on-site potential is a symmetric double-well potential.

Once its tension is adjusted, the ribbon is held tight on the top of each plate. With this precaution, the torsion constant is the same for each pendulum, and the weak residual torsional coupling between pendulums can be neglected. Each pendulum (cylinder) is attached to its neighbor with a spring. Springs connecting pendulums that are at equilibrium, in one of the bottom of a potential well, are horizontal [see Fig. 5(a)].

With the physical parameters $C_l=0$ [$l_1=l_0=68$ mm; see Eq. (23a)], $C_{\mathrm{nl}}=25$, and $k=120$, a static compacton can be observed, as represented in Fig. 5(a). The experimental shape approximately fits [see Fig. 5(b)] the theoretical shape calculated from Eq. (9).

When $C_l\neq0$ and $C_{\mathrm{nl}}\neq0$, solution (8) predicts a compacton moving at velocity $\sqrt{C_l}$ of the linear waves. In this case, we cannot conclude that the moving S-shaped entity we observe has a compact shape for the following reasons. First, we cannot control with sufficient precision the initial velocity of the kink. Second, even if we could launch a kink with exact velocity $\sqrt{C_l}$ it would gradually slow down owing to dissipative effects (that are important compared to small radiation effects predicted by our numerical simulations, see Sec. II B); thus we can never observe a moving compacton. Nevertheless, with this mechanical line we can easily observe the dynamical properties of the kinks. For example, if one launches a moving kink (unknown analytical shape) with

FIG. 5. (a) View of a static compacton on the experimental chain lying horizontally on a table. This compacton connects pendulums directed to the left (lower part of the photograph), at equilibrium in one potential well ($\Theta=-1$), to the pendulums directed to the right (upper part of the photograph), at equilibrium in the other potential well ($\Theta=+1$). (b) Comparison of the experimental static compacton shape, observed in (a) to the theoretical shape calculated from Eq. (9). Here $\Theta=\theta/\theta_m$ (with $\theta_m=\pi/3$) is dimensionless, and $X=x/a$ (with $a=10$ cm) is dimensionless; the vertical lines represent the experimental precision.

arbitrary initial velocity at one end of the line, after reflection at the opposite free end this kink becomes an antikink moving freely in the opposite direction, and so on. Depending on its initial velocity a kink can reflect three or four times before gradually slowing down owing to dissipative effects which inevitably occur for a real mechanical line. With the above physical parameters no radiation of waves due to discretness effects are observed. Thus the continuum approximation is valid. Nevertheless, lattice effects and also the pinning of kinks can be observed by simply decreasing the stiffness of the springs; such experiments will be discussed elsewhere.

V. CONCLUDING REMARKS

We have shown analytically that, in the continuum limit, the Φ-four model with nonlinear coupling only can exhibit a static compacton solution. It presents a dynamic compacton solution traveling at the characteristic velocity of linear waves when both linear and nonlinear coupling are present. Our numerical simulations point out that, contrary to the static compacton, that is stable, the dynamic compacton is unstable: it loses its compact shape when propagating, and evolves into a kink wave form which is unknown analytically. We have also shown that compacton solutions can be calculated for other topological systems with other on-site potentials such as sinusoidal (sine-Gordon type) or double-quadratic on-site potential.

In order to observe compactons and kinks, we constructed a mechanical analog which consists of an experimental chain of identical pendulums that are nonlinearly coupled and experience a double-well on-site potential of the Φ-four type. This analog model allows us to observe, in the strong nonlinear coupling limit, static compactons. This experimental result confirms our numerical simulations results. Our experimental model is also convenient to illustrate and study qualitatively the dynamical properties of kinks that can propagate and travel back and forth along the chain. Finally, our analytical, numerical, and experimental study points out that static compactons can exist. Such strictly localized entities should play a role in the modeling of domain walls in real systems.

ACKNOWLEDGMENT

S.D. thanks Michel Peyrard for helpful discussions and comments.

APPENDIX

In this appendix we derive Eq. (21). The general equation of motion of the nth pendulum of the chain represented in Fig. 3 is

$$I\frac{d^2\theta_n}{dt^2}=-K\theta_n+mgd\,\sin\theta_n+M_{n-1,n}-M_{n,n+1},$$

where $M_{n-1,n}$ and $M_{n,n+1}$ are the torque exerted by pendulum $n-1$ on pendulum n and pendulum n on pendulum $n+1$. In terms of the components $y_n=-d\,\sin\theta_n$ and $z_n=d\,\cos\theta_n$ of the displacement, the elongation of the spring (see Fig. 3) between pendulums n and $n+1$ is

$$\Delta l=\sqrt{l_1^2+(y_{n+1}-y_n)^2+(z_{n+1}-z_n)^2}-l_0,$$

where l_0 is the length of the spring at rest, and l_1 the minimal length of the stretched spring between two pendulums. Thus we have

$$M_{n,n+1}=\frac{k\Delta l}{V}\,(y_{n+1}z_n-y_nz_{n+1}),$$

where

$$(y_{n+1}z_n-y_nz_{n+1})=d^2\,\sin(\theta_n-\theta_{n+1})$$

and

$$V=\left[l_1^2+4d^2\,\sin^2\frac{(\theta_n-\theta_{n+1})}{2}\right]^{-1/2}.$$

One obtains

$$M_{n,n+1}=kd^2\left\{1-\frac{l_0}{l_1}\left(1+\frac{4d^2}{l_1^2}\,\sin^2\frac{(\theta_n-\theta_{n+1})}{2}\right)^{-1/2}\right\}\times\sin(\theta_n-\theta_{n+1}).$$

$M_{n-1,n}$ is obtained by replacing n by $n-1$ in the above expression. When the difference between the angular displacement of neighboring pendulums is small enough (weakly discrete limit), the torques can be replaced by their expansion in terms of these angular differences, and we obtain Eq. (21).

[1] A. R. Bishop and T. R. Lewis, J. Phys. C **12**, 3811 (1979).
[2] H. J. Mikeska, J. Phys. C **11**, L27 (1978).
[3] J. Rubinstein, J. Math. Phys. **11**, 258 (1970); J. Krumhansl and J. R. Schrieffer, Phys. Rev. B **11**, 3535 (1975).
[4] R. Hobart, J. Appl. Phys. **36**, 1944 (1965).
[5] M. Peyrard and A. R. Bishop, Phys. Rev. Lett. **62**, 2755 (1989).
[6] F. Fillaux and F. Carlile, Phys. Rev. B **42**, 5990 (1990).
[7] R. D. Parmentier, in *Solitons in Action*, edited by K. Lonngreen and A. C. Scott (Academic, New York, 1978).
[8] S. Flach and K. Kladko, Phys. Rev. E **54**, 2912 (1996).
[9] F. Zhang, Phys. Rev. E **54**, 4325 (1996).
[10] P. Rosenau and J. M. Hyman, Phys. Rev. Lett. **70**, 564 (1993).
[11] P. J. Olver and P. Rosenau, Phys. Rev. E **53**, 1900 (1996).
[12] A. C. Scott, Am. J. Phys. **37**, 5261 (1969).
[13] M. Remoissenet, *Waves Called Solitons. Concepts and Experiments*, 2nd ed. (Springer, New York, 1996).
[14] R. D. Peters, Am. J. Phys. **63**, 1128 (1995).